2019-09

LongWavelength Sinuosity of Linear Dunes on Earth and Titan and the Effect of Underlying Topography

Telfer, MW

10.1029/2019je006117
Journal of Geophysical Research: Planets
American Geophysical Union (AGU)

Long Wavelength Sinuosity of Linear Dunes on Earth and Titan and the Effect of Underlying Topography

M. W. Telfer[1], J. Radebaugh[2], B. Cornford[3] and C. Lewis[2]

[1]. School of Geography, Earth and Environmental Sciences, Plymouth University, Drake Circus, Plymouth, Devon, UK, PL4 8AA.

[2]. Department of Geological Sciences, College of Physical and Mathematical Sciences, Brigham Young University, Provo, UT 84602, USA.

[3]. Formerly of School of Geography, Earth and Environmental Sciences, Plymouth University, Drake Circus, Plymouth, Devon, UK, PL4 8AA.

Corresponding author: Matt W. Telfer (matt.telfer@plymouth.ac.uk)

Key Points:

- Local variations in dune trend are identified in some linear dunefields on Earth and Titan.
- The cause is identified as underlying topographic relief resulting in down-slope deflection of dunes.
- Dunefield patterning offers the potential to infer topographic relief, with implications for identifying planetary lander sites.

Abstract

On both Earth and Titan, some linear dunefields are characterized by curvilinear patterning atypical of the regularity and straightness of typical longitudinal dunefields. We use remotely sensed imagery and an automated dune crestline detection algorithm to analyze the controls on spatial patterning. Here it is shown that topography can influence the patterning, as dune alignments bend to deflect downslope under the influence of gravity. The effect is pronounced in a terrestrial dunefield (the Great Sandy Desert, Australia) where substantial topography underlies, but absent where the dunefield is underlain by subdued relief (southwestern Kalahari). This knowledge allows the inference of subtle topographic changes underlying dunefields from dunefield patterning, where other sources of elevation data may be absent. This methodology is explored using the Belet Sand Sea of Titan, and likely areas of topographic change at resolutions finer than those currently available from radar altimetry are inferred.

Plain Language Summary

Linear dunes form large dunefields both on Earth and Saturn's moon Titan, and look remarkably similar on both worlds. They are characterized by repeated ridges of sand which extend approximately parallel to the wind, and may continue unbroken for tens or even hundreds of kilometers. Perhaps their most remarkable feature is their regularity, and consistent orientation of the dunes. In a few locations, however, the dunes form distinctive curved patterns. This study investigates the causes of this phenomenon, by comparing two dunefields on Earth; Australia's Great Sandy Desert, where the curved dunes are abundant, and the Kalahari of southern Africa, where they are absent.

The cause of the curved dunes is shown to be underlying topography. The Kalahari is very flat, and thus the dunes form straight lines. But the Great Sandy Desert lies over a long-dry river valley system, and where the dunes encounter slopes, the deflect downslope. On Titan, knowledge of surface elevations and topography is patchy, and with lander missions planned better understanding is important. The method of analysis proposed here is demonstrated on radar data from the Belet dunefield of Titan, and we show that topography can be inferred from dune patterning alone.

1 Introduction

Accurate determination of surface topography is crucial for the success of planetary landers (e.g. Braun & Manning, 2007; Golombek et al., 1997; Striepe et al., 2006; Witte et al., 2016). Although final guidance is typically done autonomously (e.g. using LiDAR; Johnson et al., 2002), initial site selection remains crucial if hazard avoidance is to be maximized. This is often hampered by a lack of high-resolution imaging and/or topographic data of a world's surface, perhaps best illustrated by the design of the Huygens lander for Saturn's moon Titan as part of the Cassini-Huygens mission, given that at the time of launch it was unclear whether the landing would be on a solid or liquid surface (Zarnecki et al., 2005). The fact that the surface was revealed during the descent of the lander not only to be solid, but topographically complex (Soderblom et al., 2007), makes the successful landing even more remarkable. The continued Cassini Prime, Equinox, Solstice and Grand Finale missions (2005-2017) included a total of 127 Titan close flybys, and yet the most robust published elevation model for Titan (Corlies et al., 2017), based on radar altimetry, radar SAR and photogrammetry, is still based on just 9.2% coverage, with the rest interpolated. Both for reasons of understanding geological processes (Corlies et al., 2017), but also in the light of future exploration of Titan (Lorenz et al., 2017; Turtle et al., 2018), better understanding of Titan's topography is needed.

Linear dunes (that is, dunes forming approximately longitudinal to the net sand-moving winds; Fryberger & Dean, 1979; Lancaster, 1982; Tsoar, 1983) are the most abundant desert dune type on Earth (Lancaster 1989; Lancaster, 1995). They also form the most extensive dune system in the solar system as an equator-encircling belt on Titan covering as much as 15% of the body (Lorenz & Radebaugh, 2009; Lorenz et al., 2006; Radebaugh et al., 2008; Radebaugh et al., 2010). Whether linear dunes align with the net annual sand transporting wind (McKee, 1979), to maximize the net annual sand transport across the crest of the dune (Rubin & Hunter, 1987), or if there is a supply-limited control on their orientation (du Pont et al., 2014; Ping et al., 2014) is debated. Their remarkable regularity and consistency in terms of orientation, relief and spacing across distances of 1-10^3 km distinguish them; "Earth has no landform more regular and extensive" (Cooke et al., 1993; p.374). Typically, this regularity is expressed in landforms which, on Earth, are 5 – 120 m high, extend for 10 – 100 km, are regularly spaced on the order of 500 – 5000 m, and which typically occur in groupings of up to 1000 with orientations deviating by only a few degrees over the course of 100s of km (Fig. 1a, 1b; Lancaster, 1995). On Titan, an estimated 2×10^5 km^3 of organic material is distributed in the equatorial belt of linear dunes, typically approaching ~100 m high where measurements are possible, and similarly arranged in regular, repeated patterns of hundreds of adjacent dunes (Lorenz et al., 2008; Lorenz & Radebaugh, 2009; Lorenz et al., 2006; Radebaugh et al., 2008; Rodriguez et al., 2014).

Although linear dunes are characterized by their regularity and organization relative to the regional wind regime, their orientation and planform patterning can also be influenced by obstacles within the dunefield. On both Earth (Fig 1c) and Titan (Fig 1d) dunes are seen to reorient themselves upwind of topographic obstacles. This topographic steering is well-reported for terrestrial coastal dunes (e.g. Bauer et al., 2012; Walker et al., 2009), and the mechanism relates to feedbacks with the deformable bed and boundary layer which propagate upwind (Wilson, 1972), by which bedforms may be deflected even kilometres upwind of the obstruction to sediment transport.

In some dunefields, however, a singular, preferential orientation of the dunes is less pronounced; the dunes' orientation over a given region, whilst spacing remains regular, is more complex. This effect is seen in areas of the Great Sandy Desert of northwestern Australia (Fig. 1e), as well as the Australian Great Victoria Desert (Hesse, 2010; 2011) and is also observed on some of Titan's dunefields (Fig. 1f). In both of these cases, the dunes have a pronounced, large-scale curvilinear patterning in planform, resulting in long-wavelength (~10-100 km) sinuosity of the dunes without obvious topographical obstructions causing the deflections in patterning (Lucas et al., 2015), as well as the continental-scale (100-1000 km) curvature shown by some dunefields relating to synoptic-scale changes in typical wind regime (e.g. Hesse, 2010; Lancaster, 1981). There is, however, pronounced variability in the topography underlying the Great Sandy Desert, and it is this topographical influence that we seek to investigate. This paper thus aims to 1) investigate the causes of broad-scale linear dune curvilinearity in the terrestrial setting, and 2) explore the analogue inferences that can thus be derived for Titan's dunefields. We do this by investigating 1) the Great Sandy Desert of western Australia, where locally curvilinear duneforms are found, 2) the southwestern Kalahari, where a regional shift in linear dune orientation exists but localized variability is absent and 3) the Belet Sand Sea on Titan, where localized shifts in dune orientation are apparent. This enables us to deduce the topographic influences on different terrestrial dunefields and to explore the likely inferences for planetary topography that can be interpreted from dunefield patterning.

2 Materials and Methods

We use the Aster GDEM (NASA/METI, 2001), and Landsat8 RGB (Red:Green:Blue – Bands 4-2) and panchromatic data (Band 8), to analyse a) a region of the Great Sandy Desert in northwestern Australia, between 19 - 21°S and 122 - 125°E, b) the southwestern Kalahari of southern Africa, between 24 - 27°S and 19-21 °E. All analysis was performed within ArcGIS 10.3. The Linear Dune Oriented (LIDO) algorithm presented by Telfer et al. (2015) was used on the 15 m resolution panchromatic Band 8 data to define dune crestlines based on changes in image brightness apparent at the crests of the dunes. A pan-sharpened RGB composite was used for validation of the automated classification of crestlines. Full methodological details of the algorithm, its accuracy and precision, and details of the images used are provided in Telfer et al. (2015) and in the Supplementary Material, but in summary, the routine uses a pair of 5x5 Sobel operators on the panchromatic image to derive gradient magnitude and direction. These are used to identify reflectance gradients within ± 45° of the modal direction (which correspond to dune crest orientation), and the reflectance gradient magnitude is then used to define candidate crestline pixels. In this instance, the recursivity of defining strong and weak candidate dune crest-line zones proposed in Telfer et al. (2015) was not found necessary, and pixels were included where the gradient magnitude exceeded $\mu + (1.25 \times \sigma)$ (where μ is the mean reflectance, and σ the standard deviation). Resultant zones of less than 4500 m^2 were excluded to reduce noise, and candidate pixels were then vectorized using ArcGIS's ArcScan tool (see Supplementary Material for details of the settings employed). Only vectorized crestline sections in excess of 1 km length were considered for further analysis to further reduce noise. ArcGIS's Linear Directional Mean tool was used to derive a regional average orientation for the dunes, and the variation of individual dunes from this mean was subsequently classified using the Natural Breaks method with Jenks optimization within ArcGIS.

For the Belet dunefield of Titan, we use a mosaic of the equatorial, trailing hemisphere T8 and T61 Cassini Synthetic Aperture RADAR (SAR) swaths. These offered a pixel size of approximately 180 × 180 m. The study area extends from latitudes -5.6° to -10.2°– -12.3° and longitudes 108.7° to 124.3°; a total area of approximately 180,000 km^2. The dunes on Titan are characterized by a change in their 2.17 cm SAR reflectance relative to the surrounding terrain, with dunes being SAR-dark and underlying materials, and sometimes crestline reflections, being SAR-bright, similar to 3-cm SAR observations of fine dune sand on Earth. This, together with presence in some areas of apparently sandy interdunes and relatively poor image resolutions, means that rather than observing the change in visible light at the crestline (i.e. the contrast between illuminated and shadowed flanks of the dunes), we note that we are likely to be mapping the dune/interdune margin (e.g. Savage et al. 2014). Nonetheless, examples of the resultant digitization (see Supplementary Material) suggest that the routine accurately captures overall trends at the scales investigated here. The LIDO algorithm was again used to define dune trendlines, although the different characteristics of the SAR observations necessitated some modification of the protocol. Due to the noisier nature of the Cassini SAR data compared to the Landsat images, a 3 × 3 low-pass filter was applied initially to reduce the influence of unduly SAR-bright pixels. This was then passed with the same pair of Sobel operators, from which gradient magnitude and direction were calculated. Despite clear visual differentiation of many of the dunes, the strength of the gradient was highly variable on a pixel-by-pixel basis, and a relaxed criterion of $\mu - (0.25 \times \sigma)$ sigma was required. Combined with a slightly widened criterion for inclusion in terms of gradient direction (± 60° of the mode), suitable delineation of dune sections was achieved. Once again, relatively small candidate zones were removed (< 1.6

167 km^2) and trendlines vectorized with ArcScan. Reflecting the lower resolution of the SAR data,
168 only sections longer than 3 km were included for further analysis.

169 **3 Results**

170 *3.1 Great Sandy Desert*

171 The LIDO algorithm identified a total of 44 823 crestline sections in excess of 1 km in length
172 (mean = 2.14 km, standard deviation = 1.36 km, maximum = 39.70 km) for the studied sector of
173 the Great Sandy Desert. This region epitomizes the long-wavelength, sinuous linear dunes, and is
174 topographically characterized by a broad E-W drainage in its northern half (the Mandora
175 palaeodrainage (Tapley, 1988; Wyrwoll et al., 1986); the catchment is currently dry), with ~230
176 m relief, and highlands (~250 m elevation) in the south (Fig. 2a). The dunes propagate
177 essentially westwards under the influence of easterly net sand-transporting winds associated with
178 the continental anticyclone (Hesse, 2010; Kalma et al., 1988). Linear dunes (Fig. 2b) are widely
179 distributed across the region, and do not show clear regional trends in abundance, though there
180 are, as is common in linear dunefields, some localized groupings of dunes, especially in the
181 southern part of the study area. However, when the deviation of individual dune orientation is
182 calculated against the regional mean (roughly E – W: 281.4°; Fig. 2c), a relationship with the
183 topography (Fig. 2a) becomes apparent. When the deflection from Fig. 2c is averaged to a 5km
184 grid (Fig. 3a), the zonal nature of the local reorientation of the dunes can be clearly seen, and is,
185 in, part, related to landscape roughness, in this case the standard deviation of elevations from
186 Fig. 2a over a 5 km grid (Fig. 3b). However, it is when the slope orientation, derived from the
187 regional elevation data from Fig. 2a and gridded to 5 km squares, shown as arrows in Fig. 3c, is
188 shown against the 5 km gridded dune deflection (3a) that the true nature of the relationship
189 becomes apparent (Fig. 3c). Dunes deflect northwards (red colors) when the slope descends
190 towards the north, and southwards (blue) in the case of south-dipping slopes. Given the westward
191 propagation of the dunefield, dunes deflect downslope when obliquely encountering both rising
192 and falling topography.

193 *3.2 Southwestern Kalahari*

194 The studied sector of the southwestern Kalahari dunefield occupies a broad swathe of dunes
195 trending approximately NNW-SSE, and the LIDO algorithm identified 30 782 crestline sections
196 in excess of 1 km in length. The topography of the region is very subdued (Fig. 4a) and has
197 indeed led to the coining of the term 'geomonotony' (Eckhardt, 2010); dunes are on the order of
198 8 – 10 m in elevation, and the few dry valleys that dissect the dunes are typically broad (~10 km)
199 and shallow (~30 m). Deviations to the mean regional trend of the dune crestlines are limited to a
200 shift from north-south trending at the northern end of the study area to northwest-southeast
201 trending at the southern edge of the dunefield (Fig. 4b and 4c). This overall pattern is well-
202 reported, and typically associated with the southern African continental anticyclone (Lancaster,
203 1980; Lancaster, 1981; Lancaster, 1988). Although some very localized reorganisation of pattern
204 and orientation in the vicinity of dry valleys is apparent along the Auob and Nossop river valleys
205 (Fig. 4a; Bullard & Nash, 1998, 2000), in general, the zonal variability evident in the Great
206 Sandy is absent here. Similarly, no clear relationship exists between the deflection of the dunes
207 (Fig. 5a) and the minimal landscape roughness (Fig 5.b), or the low-relief slopes evident
208 throughout the dunefield (Fig. 5c). Only in a small region adjoining the Nossob catchment in the

far north of the study region does enhanced topography coincide with local deflection of the dunes at the scale investigated here.

4 Discussion

The findings presented in the preceding section can be summarized; where substantial topographic variation exists beneath a linear dunefield, it can result in downslope deflection of the dunes and disruption of the regional pattern. This effect is quantified in Figure 6. For the Great Sandy Desert, with its substantial (~200 m) local variation in topography, there is a strong correlation between the incidence angle between the dunes and the underlying slope, and the resultant deviation from the regional mean trend of the dunes (Fig. 6a). This correlation is further increased (Fig. 6b) when the incident angle of the dune trend/slope angle is weighted by the magnitude of the slope; that is, steeper local slopes seem to deflect dunes more than shallow gradients. The magnitude of the deflection of the dune is maximized when the dune/slope intercept reaches 90° (that is, when the dune trend is orthogonal to the local slope). By contrast, for the Kalahari, with its low relief underlying the dunefield, no such correlation is apparent, either unweighted (Fig. 6c) or weighted (Fig. 6d). Although the effect is seen here manifested around a large valley system, the presence of deflection even on dunes extending up slopes implies that similar effects are likely on positive relief.

A number of possibilities exist for the mechanism controlling this effect. Because, by definition of their topographic expression, aeolian entrainment and deposition on dune surfaces is rarely on horizontal, flat surfaces, the influence of slope on aeolian processes has been studied using numerical modelling (e.g. Tsoar et al., 1996; White & Tsoar, 1998), computational fluid dynamics (Fariaet al., 2011; Huang et al., 2008) and wind tunnel experimentation (Bullard & Nash, 1998; Bullard et al., 2000; Iversen & Rasmussen, 1994, 1999; White & Tsoar, 1998). Few studies have focussed at the landform scale, and fewer still consider the role of oblique slopes. However, wind tunnel experimentation has suggested that the net result of oblique winds incident to a valley is the deflection of the wind along the valley (i.e. in the opposite direction to that observed here for downward slopes) (Bullard and Nash, 2000; Garvey et al., 2005). This suggests that a mechanism other than simple topographic steering of winds along valleys is necessary to explain the observations.

Two possibilities are suggested here for a mechanism by which the dunes are deflected downslope. Firstly, it may simply be a gravitational effect, as whether dunes are descending or ascending incident oblique slopes, the deflection is downhill. Whilst gravity-driven (that is, katabatic) winds are known to be influenced by topography (e.g. Nylen et al., 2004), it is also possible that gravitational effects would also presumably affect individual transported grains by preferential settling on deposition from aeolian transport downslope; on deposition, grains might roll downhill, but will not roll uphill. Extrapolated to the landform scale, the result would be the deflection of the dune crestline down the slope. Alternatively, it may be that the effect of the valley on the localized wind regime acts in a manner analogous to that known to occur over positive topographic features, such as coastal foredunes. Here, the effect of topography in steering incident winds towards the normal direction of the crestline is well described (reviewed in Hesp et al., 2015), and results from the pressure gradient force resulting from differential flow acceleration associated with oblique incident winds. Whilst the impacts of such topographic steering have predominantly been studied on dunes transverse to the net air flow, it is possible

that pressure-driven force associated with flow separation could deflect the linear dunes. Such effects have been modelled using wind tunnels and differing geometries of valley (Bullard et al., 2000), and whilst it was generally observed that the effect of negative topography was the steering of streamlines along the valley line (i.e. the opposite direction to that observed here), it is also noted that the effects are a function of a complex set of variables including valley geometry, thermal stability of the airmass and wind regime. Further study is needed to disentangle the relative roles of gravity-driven mechanisms and possible localized effects of topography on the wind regime in realigning the dunes.

These results suggest a method for identifying topography from dunefield patterning where no such elevation data might otherwise be sparse, or missing, at the relevant scale. Here we apply the dune trendline detection method to the Belet dunefield on Titan, where similar curvilinear dune patterning to that observed in the Great Sandy Desert is present. The studied region consists of a broad belt of west-east trending dunes (sand transport direction inferred to be eastward from dune interactions with obstacles; Radebaugh et al. 2010) with several radar-bright obstacles interrupting the patterning, and a dark, largely dune-free corridor to the southeast of the images. The LIDO algorithm identifies 5322 dune sections of at least 3 km length within the studied region, with a radial mean orientation of 79°.

When the deviation in the dune orientations from the regional mean is considered (Figure 7a), the superficial similarity with the Great Sandy Desert is further supported. Unlike in the Kalahari, variation in dune orientation occurs at a relatively local scale. In some instances (Figure 7b), such as in the far northwest of the studied area, these deviations are clearly adjacent to radar-bright gaps in the dune sands, and this effect is both well-reported (Ewing et al., 2015; Lorenz et al., 2006; Radebaugh et al., 2008; Radebaugh et al., 2010; Savage et al., 2014), and likely to be due to deflection of dunes around obstacles (i.e. mountains or hills) standing proud of the dunefield. But in other areas, localized variance in dune trendline is not obviously associated with obstacles, and thus we propose that this is likely the result of underlying topography at a scale not observed by Cassini SAR and radar altimetry data. The resultant likely topographic trends are illustrated in Figure 7b, and are likely to be at a scale more subtle than that observable from the Titan Digital Elevation Model (DEM) (Corlies et al., 2017). While some lineations in the southern and eastern part of the image can still be observed but not selected by the LIDO algorithm, it is tempting to suggest that at least a portion of that corridor is, in the light of its morphology and the inferred slopes down into this region, a fluvial or relic fluvial valley (Birch et al., 2016; Burr et al., 2013; Jaumann et al., 2008; Langhans et al., 2012; Lorenz et al., 2008). It is also possible that small-scale (i.e. individual dune) deflections evident in some parts of the studied area are indicative of localized dune trends, but further work is needed to confirm this. Such information may prove valuable in planning lander sites for future missions to Titan, as it offers additional information regarding the surface of potential landing sites and their surface topography. In addition to the likely increase in surface roughness associated with fluvial erosion creating local topographic relief, it is also likely that Titan's fluvial channels, especially those that are radar-bright, may have increased frequency of fluvially-derived clasts (Burr et al., 2013), an additional hazard for planetary landers.

It has been noted that despite the differences of Titan's different atmospheric density (146 KPa, or 145% that of Earth), gravity (1.35 m s^{-2}, or 14% that of Earth) and likely particle density (0.4-1.5 g cm^{-3}, or 15-55% that of Earth's silicate sands), the similarity of the resultant aeolian

landforms to terrestrial dunes is striking (Lorenz et al., 2006). The presence of curvilinear longitudinal dune forms is further evidence of this similarity. It is possible that their presence on Titan, given the low gravity and very low particle/fluid density ratio (Burr et al., 2015), might favour pressure-gradient mechanisms.

5 Conclusions

We investigate the properties of linear (longitudinal) dunefields where the typically highly-consistent orientation of dunes is less pronounced, and curvilinear, long-wavelength sinuosity is apparent. Such patterning is scarce on Earth, but relatively common on Titan. We show that on Earth, such patterning results from underlying topography causing the dunes to deflect downslope as they form and propagate. The effect is maximized as the incidence angle between the dunes and the slope approaches 90°, and is further shown to be dependent on the gradient of the slope, with steeper slopes resulting in more pronounced deflection. Dune morphometry thus offers an additional source of information regarding local and regional topography where such information is scarce, as is the case for some planetary dunefields. The mechanism by which the dunes are deflected likely relates to either gravity-driven processes affecting either the airflow or settling grains, or by local pressure gradients related to airflow separation; the presence of the curving dunes even in Titan's low gravity may favour the latter. We demonstrate the potential of this method to infer topography in a region of the Belet Sand Sea in Titan's equatorial belt, and suggest it offers the potential to increase topographic understanding of the surface of Titan both for geological purposes and in terms of identifying optimal lander sites for future missions. To find the lowest relief areas amongst the dunes, future landers would be best guided away from areas where dunes demonstrate long-wavelength sinuosity.

Acknowledgments, Samples, and Data

There are no real or perceived financial conflicts of interests for any author, nor other affiliations for any author that may be perceived as having a conflict of interest with respect to the results of this paper.

Landsat8 data are freely available from the U.S. Geological Survey. ASTER GDEM is a product of NASA and METI. The T8 and T61 Cassini radar data set was obtained from the Planetary Data System (PDS). Detail of the LIDO workflow used within ArcGIS is provided in the Supplementary material.

MT and BC have no funding sources related to this work to declare. JR and CL were funded in part by the NASA Space Grant Program.

References

Bauer, B. O., Davidson-Arnott, R. G. D., Walker, I. J., Hesp, P. A., & Ollerhead, J. (2012). Wind direction and complex sediment transport response across a beach-dune system. *Earth Surface Processes and Landforms, 37*(15), 1661-1677. doi:10.1002/esp.3306

Birch, S. P. D., Hayes, A. G., Howard, A. D., Moore, J. M., & Radebaugh, J. (2016). Alluvial Fan Morphology, distribution and formation on Titan. *Icarus, 270*, 238-247. doi:10.1016/j.icarus.2016.02.013

Braun, R. D., & Manning, R. M. (2007). Mars exploration entry, descent and landing challenges. *Journal of Spacecraft and Rockets, 44*(2), 310-323. doi:10.2514/1.25116

Bullard, J. E., & Nash, D. J. (1998). Linear dune pattern variability in the vicinity of dry valleys in the southwest Kalahari. *Geomorphology, 23*(1), 35-54.

Bullard, J. E., & Nash, D. J. (2000). Valley-marginal sand dunes in the south-west Kalahari: their nature, classification and possible origins. *Journal of Arid Environments, 45*(4), 369-383.

Bullard, J. E., Wiggs, G. F. S., & Nash, D. J. (2000). Experimental study of wind directional variability in the vicinity of a model valley. *Geomorphology, 35*(1), 127-143. doi:https://doi.org/10.1016/S0169-555X(00)00033-7

Burr, D. M., Perron, J. T., Lamb, M. P., Irwin, R. P., Collins, G. C., Howard, A. D., . . . Black, B. A. (2013). Fluvial features on Titan: Insights from morphology and modeling. *Geological Society of America Bulletin, 125*(3-4), 299-321. doi:10.1130/b30612.1

Burr, D. M., Bridges, N. T., Marshall, J. R., Smith, J. K., White, B. R., & Emery, J. P. (2015). Higher-than-predicted saltation threshold wind speeds on Titan. *Nature, 517*(7532), 60.

Cooke, R. U., Warren, A., & Goudie, A. S. (1993). *Desert Geomorphology*. London.: University College Press.

Corlies, P., Hayes, A. G., Birch, S. P. D., Lorenz, R., Stiles, B. W., Kirk, R., . . . Iess, L. (2017).

Titan's Topography and Shape at the End of the Cassini Mission. *Geophysical Research Letters, 44*(23), 11754-11761. doi:10.1002/2017gl075518

du Pont, S. C., Narteau, C., & Gao, X. (2014). Two modes for dune orientation. *Geology, 42*(9), 743-746. doi:10.1130/g35657.1

Eckhardt, F. (2010). Hydrogeology. In Centre for Applied Research and Department of Environmental Affairs (Ed.), *Makgadikgadi Framework Management Plan* (Vol. Volume 2). Gaborone, Botswana: Centre for Applied Research and Department of Environmental Affairs.

Ewing, R. C., Hayes, A. G., & Lucas, A. (2015). Sand dune patterns on Titan controlled by long-term climate cycles. *Nature Geoscience, 8*(1), 15-19.

Faria, R., Ferreira, A. D., Sismeiro, J. L., Mendes, J. C. F., & Sousa, A. C. M. (2011). Wind tunnel and computational study of the stoss slope effect on the aeolian erosion of transverse sand dunes. *Aeolian Research, 3*(3), 303-314. doi:10.1016/j.aeolia.2011.07.004

Fryberger, S. G., & Dean, G. (1979). Dune forms and wind regime. In E. D. McKee (Ed.), *A study of global sand seas* (Vol. 1052): USGS Professional Paper.

Garvey, B., Castro, I. P., Wiggs, G., & Bullard, J. (2005). Measurements of flows over isolated valleys. *Boundary-Layer Meteorology, 117*(3), 417-446. doi:10.1007/s10546-005-2079-6

Golombek, M. P., Cook, R. A., Economou, T., Folkner, W. M., Haldemann, A. F. C., Kallemeyn, P. H., . . . Vaughan, R. M. (1997). Overview of the Mars Pathfinder Mission and assessment of landing site predictions. *Science, 278*(5344), 1743-1748. doi:10.1126/science.278.5344.1743

Hesp, P. A., Smyth, T. A. G., Nielsen, P., Walker, I. J., Bauer, B. O., & Davidson-Arnott, R. (2015). Flow deflection over a foredune. *Geomorphology, 230*, 64-74. doi:https://doi.org/10.1016/j.geomorph.2014.11.005

Hesse, P. (2011). Sticky dunes in a wet desert: Formation, stabilisation and modification of the Australian desert dunefields. *Geomorphology, 134*(3-4), 309-325. doi:10.1016/j.geomorph.2011.07.008

Hesse, P. P. (2010). The Australian desert dunefields: formation and evolution in an old, flat, dry continent. *Geological Society, London, Special Publications, 346*(1), 141.

Huang, N., Shi, F., & Pelt, R. S. V. (2008). The effects of slope and slope position on local and upstream fluid threshold friction velocities. *Earth Surface Processes and Landforms, 33*(12), 1814-1823. doi:10.1002/esp.1735

Iversen, J. D., & Rasmussen, K. R. (1994). The effect of surface slope on saltation threshold. *Sedimentology, 41*(4), 721-728. doi:10.1111/j.1365-3091.1994.tb01419.x

Iversen, J. D., & Rasmussen, K. R. (1999). The effect of wind speed and bed slope on sand transport. *Sedimentology, 46*(4), 723-731. doi:10.1046/j.1365-3091.1999.00245.x

Jaumann, R., Brown, R. H., Stephan, K., Barnes, J. W., Soderblom, L. A., Sotin, C., . . . Lorenz, R. D. (2008). Fluvial erosion and post-erosional processes on Titan. *Icarus, 197*(2), 526-538. doi:10.1016/j.icarus.2008.06.002

Johnson, A. E., Klumpp, A. R., Collier, J. B., & Wolf, A. A. (2002). Lidar-based hazard avoidance for safe landing on Mars. *Journal of Guidance Control and Dynamics, 25*(6), 1091-1099. doi:10.2514/2.4988

Kalma, J. D., Speight, J. G., & Wasson, R. J. (1988). Potential wind erosion in Australia: A continental perspective. *Journal of Climatology, 8*(4), 411-428. doi:10.1002/joc.3370080408

Lancaster, N. (1980). Dune systems and palaeoenvironments in Southern Africa. *Palaeontologia Africana, 23*, 185-189.

Lancaster, N. (1981). Palaeoenvironmental implications of fixed dune systems in southern Africa. *Palaeogeography, Palaeoclimatology, Palaeoecology, 33*, 327-346.

Lancaster, N. (1982). Linear dunes. *Progress in Physical Geography: Earth and Environment, 6*(4), 475-504. doi:10.1177/030913338200600401

Lancaster, N. (1988). Development of Linear Dunes in the Southwestern Kalahari, Southern-Africa. *Journal of Arid Environments, 14*(3), 233-244.

Lancaster, N. (1995). *Geomorphology of desert dunes*. Physical Environment Series: Routledge.

Langhans, M. H., Jaumann, R., Stephan, K., Brown, R. H., Buratti, B. J., Clark, R. N., . . . Nelson, R. (2012). Titan's fluvial valleys: Morphology, distribution, and spectral properties. *Planetary and Space Science, 60*(1), 34-51. doi:10.1016/j.pss.2011.01.020

Lorenz, R. D., Lopes, R. M., Paganelli, F., Lunine, J. I., Kirk, R. L., Mitchell, K. L., . . . Cassini, R. T. (2008). Fluvial channels on Titan: Initial Cassini RADAR observations. *Planetary and Space Science, 56*(8), 1132-1144. doi:10.1016/j.pss.2008.02.009

Lorenz, R. D., Mitchell, K. L., Kirk, R. L., Hayes, A. G., Aharonson, O., Zebker, H. A., . . . Stofan, E. R. (2008). Titan's inventory of organic surface materials. *Geophysical Research Letters, 35*(2). doi:10.1029/2007gl032118

Lorenz, R. D., & Radebaugh, J. (2009). Global pattern of Titan's dunes: Radar survey from the Cassini prime mission. *Geophysical Research Letters, 36*. doi:10.1029/2008gl036850

Lorenz, R. D., Stiles, B. W., Aharonson, O., Lucas, A., Hayes, A. G., Kirk, R. L., . . . Barnes, J. W. (2013). A global topographic map of Titan. *Icarus, 225*(1), 367-377. doi:https://doi.org/10.1016/j.icarus.2013.04.002

Lorenz, R. D., Turtle, E. P., Barnes, J. W., Trainer, M. G., Adamas, D. S., Hibbard, D. E., . . . Bedini, P. D. (2017). *Dragonfly: A Rotorcraft Lander Concept for Scientific Exploration at Titan*. Retrieved from

Lorenz, R. D., Wall, S., Radebaugh, J., Boubin, G., Reffet, E., Janssen, M., . . . West, R. (2006). The sand seas of Titan: Cassini RADAR observations of longitudinal dunes. *Science, 312*(5774), 724-727. doi:10.1126/science.1123257

Lucas, A., Narteau, C., Rodriguez, S., Rozier, O., Callot, Y., Garcia, A., & du Pont, S. C. (2015). Sediment flux from the morphodynamics of elongating linear dunes. *Geology, 43*(11), 1027-1030. doi:10.1130/g37101.1

McKee, E. D. (1979). *A study of global sand seas* (Vol. 1052). Tunbridge Wells: U.S. Government Printing Office.

NASA/METI. (2001). *ASTER L1B.*

Nylen, T. H., Fountain, A. G., & Doran, P. T. (2004). Climatology of katabatic winds in the McMurdo dry valleys, southern Victoria Land, Antarctica. *Journal of Geophysical Research-Atmospheres, 109*(D3), 9. doi:10.1029/2003jd003937

Ping, L., Narteau, C., Dong, Z. B., Zhang, Z. C., & du Pont, S. C. (2014). Emergence of oblique dunes in a landscape-scale experiment. *Nature Geoscience, 7*(2), 99-103. doi:10.1038/ngeo2047

Radebaugh, J., Loren, R. D., Lunine, J. I., Wall, S. D., Boubin, G., Reffet, E., . . . Cassini Radar, T. (2008). Dunes on Titan observed by Cassini Radar. *Icarus, 194*(2), 690-703. doi:10.1016/j.icarus.2007.10.015

Radebaugh, J., Lorenz, R., Farr, T., Paillou, P., Savage, C., & Spencer, C. (2010). Linear dunes on Titan and earth: Initial remote sensing comparisons. *Geomorphology, 121*(1-2), 122-132. doi:10.1016/j.geomorph.2009.02.022

Rasmussen, K. R., Iversen, J. D., & Rautahemio, P. (1996). Saltation and wind-flow interaction in a variable slope wind tunnel. *Geomorphology, 17*(1-3), 19-28. doi:10.1016/0169-555x(95)00090-r

Rodriguez, S., Garcia, A., Lucas, A., Appéré, T., Le Gall, A., Reffet, E., . . . Turtle, E. P. (2014). Global mapping and characterization of Titan's dune fields with Cassini: Correlation between RADAR and VIMS observations. *Icarus, 230*, 168-179. doi:https://doi.org/10.1016/j.icarus.2013.11.017

Rubin, D. M., & Hunter, R. E. (1987). Bedform Alignment in Directionally Varying Flows. *Science, 237*(4812), 276-278.

Savage, C. J., Radebaugh, J., Christiansen, E. H., & Lorenz, R. D. (2014). Implications of dune pattern analysis for Titan's surface history. *Icarus, 230*, 180-190. doi:10.1016/j.icarus.2013.08.009

Soderblom, L. A., Tomasko, M. G., Archinal, B. A., Becker, T. L., Bushroe, M. W., Cook, D. A., . . . Smith, P. H. (2007). Topography and geomorphology of the Huygens landing site on Titan. *Planetary and Space Science, 55*(13), 2015-2024. doi:10.1016/j.pss.2007.04.015

Striepe, S. A., Way, D. W., Dwyer, A. M., & Balaraim, J. (2006). Mars Science Laboratory simulations for entry, descent, and landing. *Journal of Spacecraft and Rockets, 43*(2), 311-323. doi:10.2514/1.19649

Tapley, I. J. (1988). The reconstruction of palaeodrainage and regional geologic structures in Australia's canning and officer basins using NOAA-AVHRR satellite imagery. *Earth-Science Reviews, 25*(5), 409-425. doi:https://doi.org/10.1016/0012-8252(88)90008-6

Telfer, M. W., Fyfe, R. M., & Lewin, S. (2015). Automated mapping of linear dunefield morphometric parameters from remotely-sensed data. *Aeolian Research, 19*, 215-224. doi:10.1016/j.aeolia.2015.03.001

Tsoar, H. (1983). Dynamic Processes Acting On A Longitudinal (Seif) Sand Dune. *Sedimentology, 30*(4), 567-578.

Tsoar, H., White, B., & Berman, E. (1996). The effect of slopes on sand transport — numerical modelling. *Landscape and Urban Planning, 34*(3), 171-181. doi:10.1016/0169-2046(95)00235-9

Turtle, E. P., Barnes, J. W., Trainer, M. G., Lorenz, R. D., Hibbard, K. E., Adams, D. S., . . . Ernst, C. (2018). *Dragonfly: in Situ Exploration of Titan's Organic Chemistry and Habitability*. Paper presented at the 49th Lunar and Planetary Science Conference, Woodlands, Texas.

Walker, I. J., Hesp, P. A., Davidson-Arnott, R. G. D., Bauer, B. O., Namikas, S. L., & Ollerhead, J. (2009). Responses of three-dimensional flow to variations in the angle of incident wind and profile form of dunes: Greenwich Dunes, Prince Edward Island, Canada. *Geomorphology, 105*(1-2), 127-138. doi:10.1016/j.geomorph.2007.12.019

White, B. R., & Tsoar, H. (1998). Slope effect on saltation over a climbing sand dune. *Geomorphology, 22*(2), 159-180. doi:10.1016/S0169-555X(97)00058-5

Wilson, I. G. (1972). Aeolian bedforms - their development and origins. *Sedimentology, 19*(3-4), 173-210. doi:10.1111/j.1365-3091.1972.tb00020.x

Witte, L., Roll, R., Biele, J., Ulamec, S., & Jurado, E. (2016). Rosetta lander Philae - Landing performance and touchdown safety assessment. *Acta Astronautica, 125*, 149-160. doi:10.1016/j.actaastro.2016.02.001

Wyrwoll, K. H., McKenzie, N. L., Pederson, B. J., & Tapley, I. J. (1986). The Great Sandy Desert of Northwestern Australia - the last 7000 Years. *Search, 17*(7-9), 208-210.

Zarnecki, J. C., Leese, M. R., Hathi, B., Ball, A. J., Hagermann, A., Towner, M. C., . . . Geake, J. E. (2005). A soft solid surface on Titan as revealed by the Huygens Surface Science Package. *Nature, 438*, 792. doi:10.1038/nature04211

490

491

492
493

494 **Figure 1**. Linear dunes are typified by remarkably regular planform patterning, with dunes
495 aligned approximately parallel to the net sand-transporting regional winds. Examples from a) the
496 Simpson Desert, Australia and b) the southwestern Kalahari of central southern Africa highlight
497 this regularity. In the case of the Kalahari, the orientation patterns demonstrate the occasional
498 tendency of these dunefields to reflect changes in the orientation of regional-scale atmospheric
499 circulation patterns. Such dunes may reorient around topographic obstacles to sand-transporting
500 wind flow, illustrated here from c) the Libyan Sahara (23.75°N, 21.38°E) and d) the Belet
501 dunefield of Titan (from the T61 swath, Aug. 2009). Figure 1a, 1b, 1c and 1e are courtesy of
502 Google Earth/SPOT/CNRS. In some regions, however, the dunes take a curvilinear form without
503 obvious topographic obstructions causing the change to patterning, seen here in e) the Great
504 Sandy Desert of northwestern Australia and f) the Belet dunefield (from T8, October 2005).

505 **Figure 2.** Topographic data and dune alignment for the Great Sandy Desert. a) The relief of the
506 Great Sandy Desert, b) Dune crestlines as determined by the LIDO automated detection routine,
507 and c) the deflection of the dune orientations relative to the regional mean (red = northwards;
508 blue = southwards), which highlights the localized nature of the pattern deviation. Net sand
509 transport is east-west.

510 **Figure 3.** The influence of relief on the orientation of sand dunes in the Great Sandy Desert. a)
511 shows the deviation in the regional directional trend from 2c shown here as 5 km-gridded means;
512 b) landscape roughness (here calculated as the standard deviation of elevations within a 5 km
513 grid) can be seen to closely resemble the pattern of dune deflection; c) the relative orientation of
514 the slope (arrows point downslope and are scaled by gradient) correlates most closely with the
515 deflection of the dunes (see Fig. 6).

516 **Figure 4.** Topographic data and dune alignment for the Kalahari. a) The relief of the
517 southwestern Kalahari, whilst showing greater regional changes than the Great Sandy, has much
518 more subdued local expression of relief. b) The dunes occur in a broad swathe with net sand-
519 transporting wind from the north-northwest and c) deviations in the dune crestline orientations,
520 unlike the Great Sandy, do not show pronounced local variation (cf Figure 2c), but instead reflect
521 large-scale regional changes.

522 **Figure 5.** The influence of relief on the orientation of sand dunes in the Kalahari. a) The
523 southwestern Kalahari's regional trend in dune orientation is largely independent of the relief,
524 and b) the topographic roughness (again, shown as standard deviations of elevation around a 5
525 km downsampled grid of the Aster GDEM v2.0 data) is much lower throughout the dunefield.
526 The higher relief mountains in the southwestern corner of the image are beyond the dunefield
527 limits. c) The magnitude and orientation of local slopes again highlights the lower relief apparent
528 here.

529 **Figure 6.** The relationship between the deflection of the dunes and the incident slope angle is
530 dependent upon the degree of underlying topography. a) The deflection of the Great Sandy's
531 dunes from the regional mean (approximately east-west; 280.4°) plotted as a function of the
532 relative orientation of the 5 km gridded local slope, and b) the same data, but weighted according
533 to the magnitude of the gradient. Here a cubic fit is used to reflect the likely maximum deflection
534 as slope incidence approaches +/- 90°. By contrast, no trend is apparent for the low-relief
535 southwestern Kalahari, with the data either c) unweighted or d) weighted.

536 **Figure 7.** The orientations of dune section at the eastern end of the Belet dunefield, as
537 determined reveals some dune deviations attributable to deflection around obstacles, but also
538 some which are not apparently associated with this mechanism. a) The dune trends mapped as
539 deviations from the regional mean with major radar-bright obstacles highlighted in white, and b)
540 annotated inferences reveal deviations likely due to not just topographic obstacles to airflow
541 (white arrows), but also those likely due to underlying topography. Here, the inferred
542 topographic trend is illustrated with a black arrow pointed downslope. These reveal details of
543 topography not apparent from either c) the Imaging Science Subsystem (ISS) imagery or d) the
544 derived elevation model data product (here from Lorenz et al., 2013).

Figure 1.

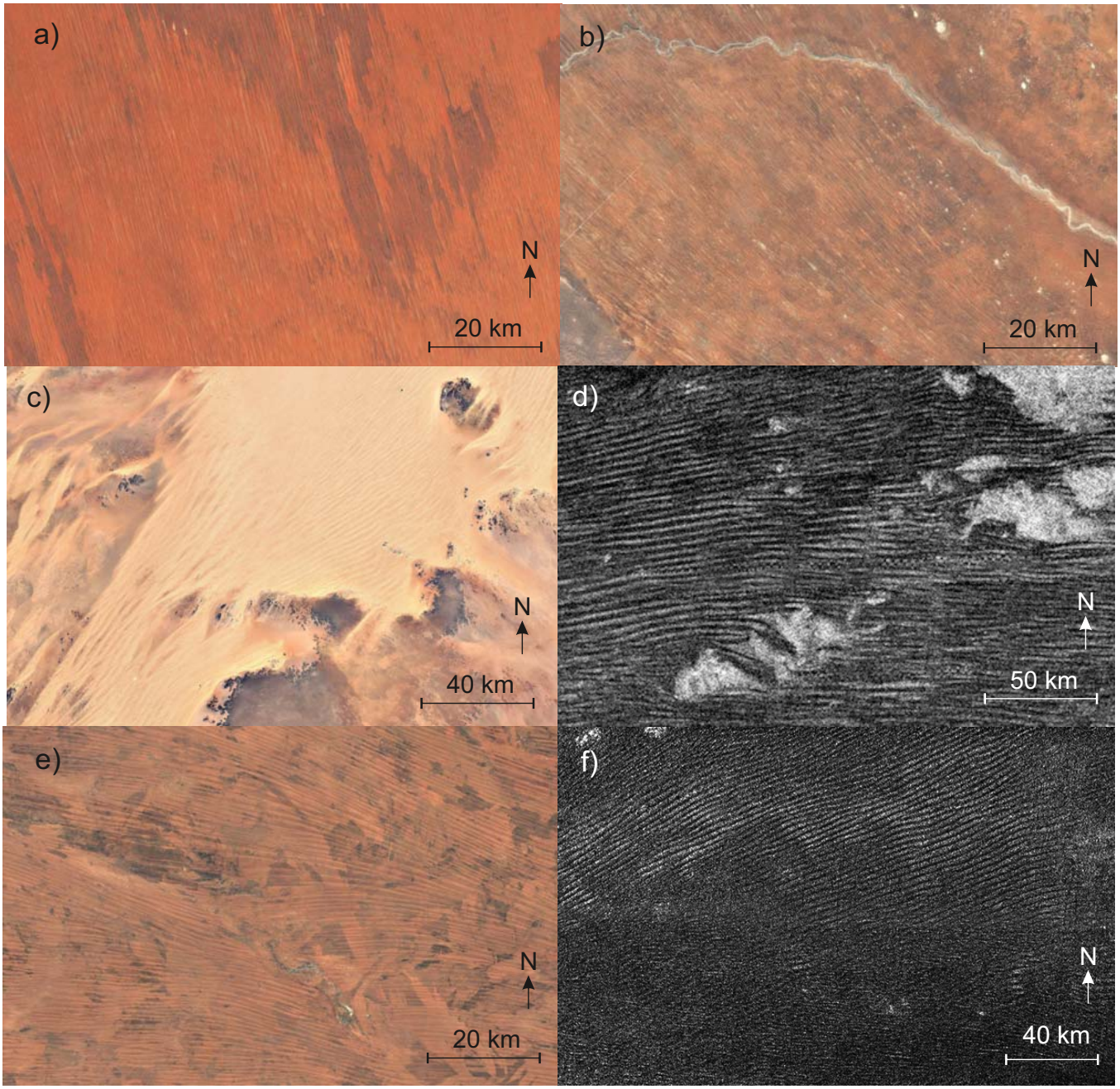
a)
N
20 km
b)
N
20 km
c)
N
40 km
d)
N
50 km
e)
N
20 km
f)
N
40 km

Figure 2.

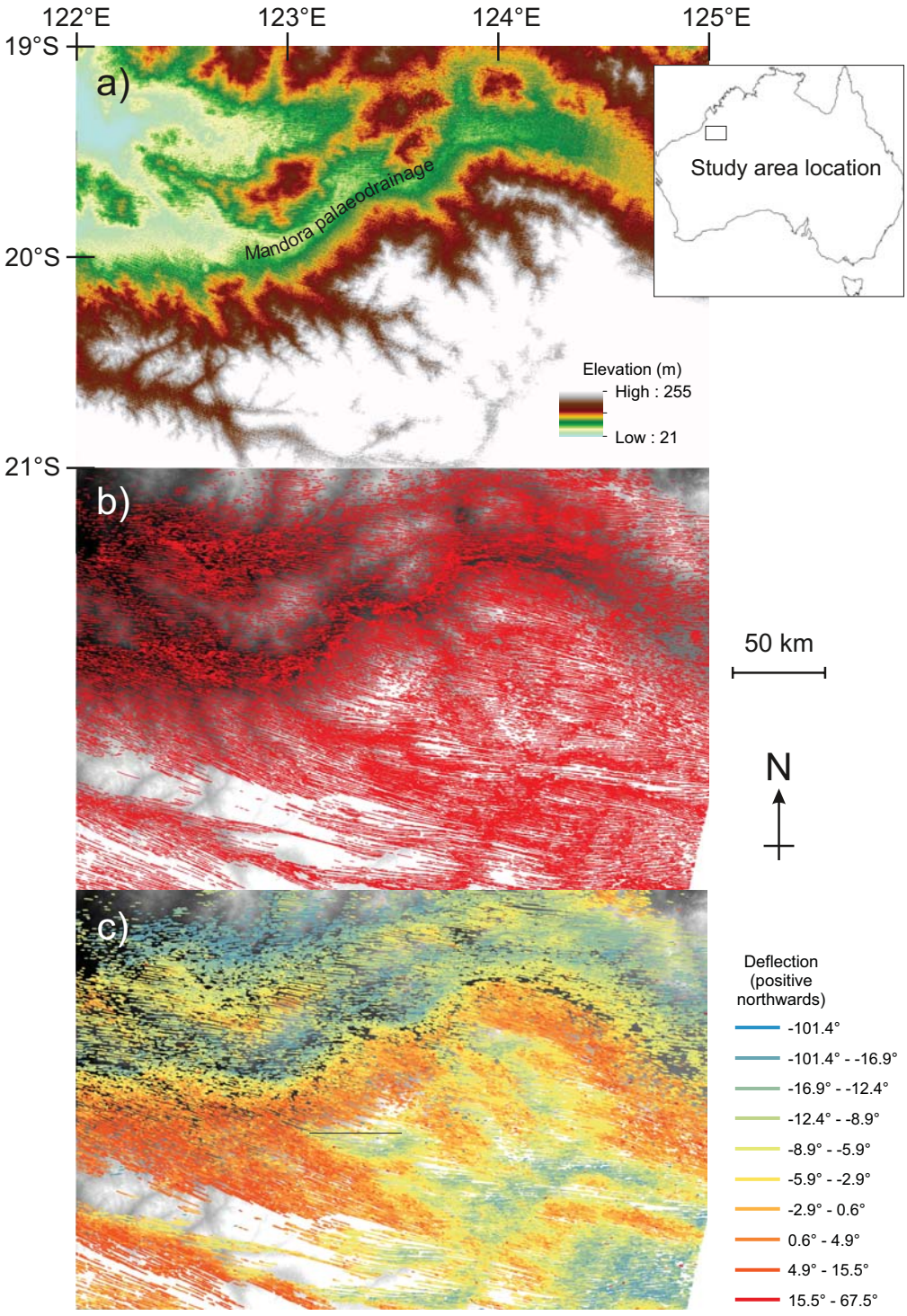
122°E
123°E
124°E
125°E
19°S
20°S
21°S
a)
Mandora palaeodrainage
Study area location
Elevation (m)
High : 255
Low : 21
b)
50 km
N
c)
Deflection
(positive
northwards)
-101.4°
-101.4° - -16.9°
-16.9° - -12.4°
-12.4° - -8.9°
-8.9° - -5.9°
-5.9° - -2.9°
-2.9° - 0.6°
0.6° - 4.9°
4.9° - 15.5°
15.5° - 67.5°

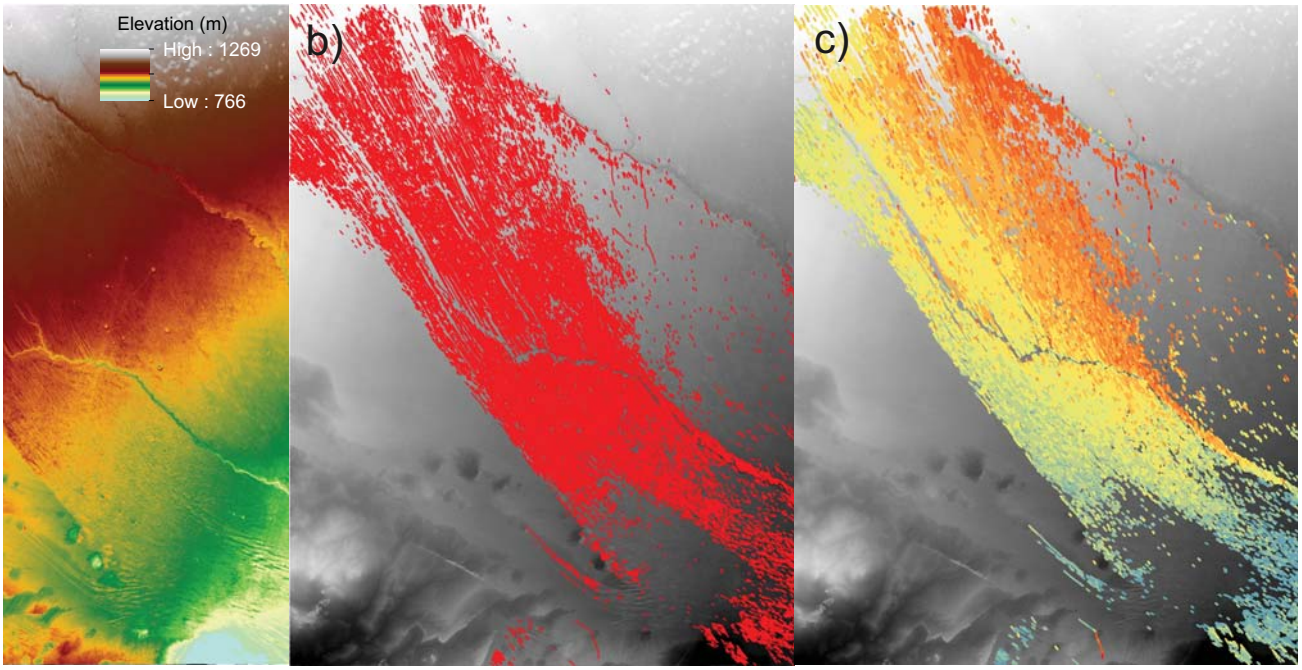
Elevation (m)
High : 1269
Low : 766
b)
c)

Figure 3.

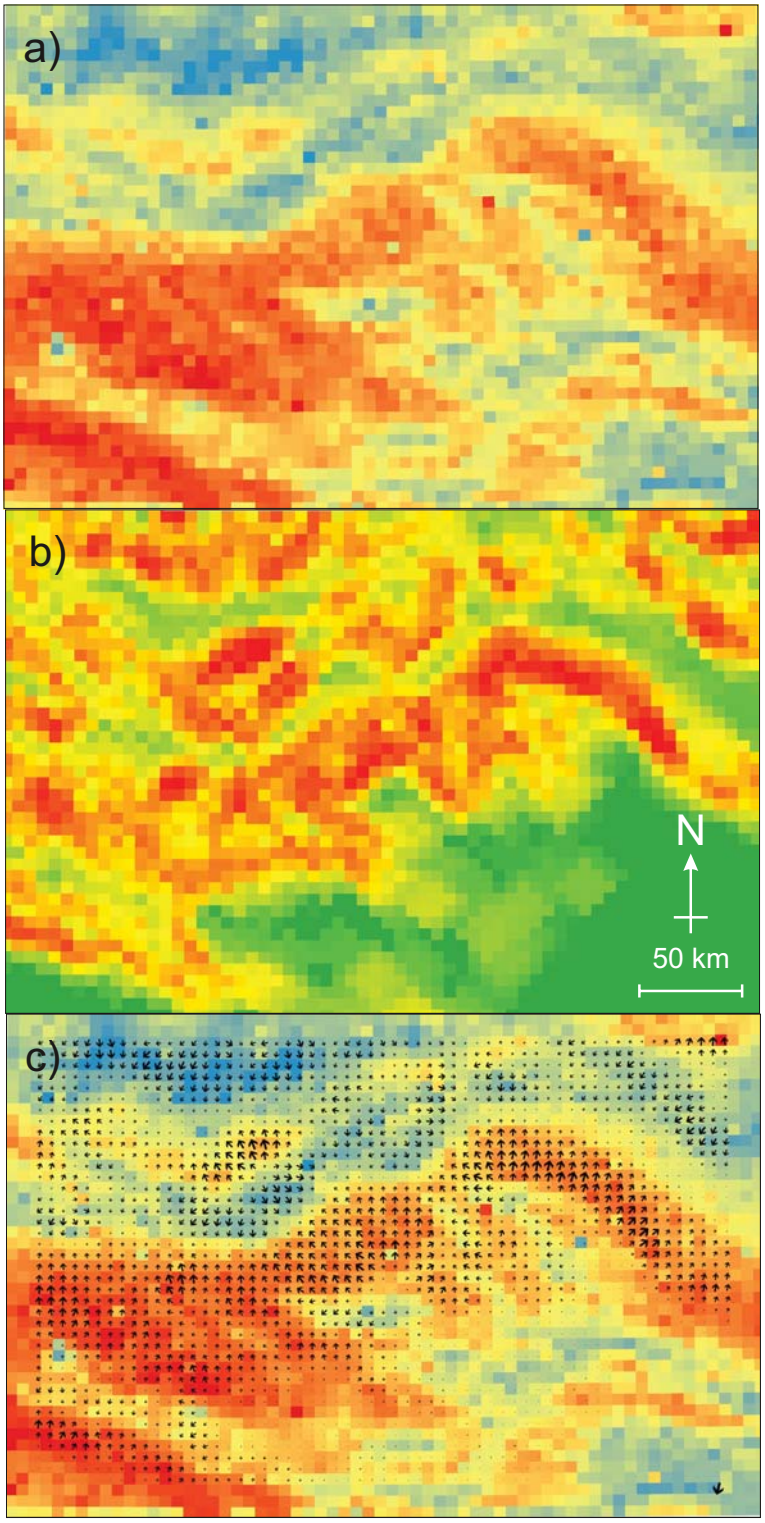
a)
b)
N
50 km
c)

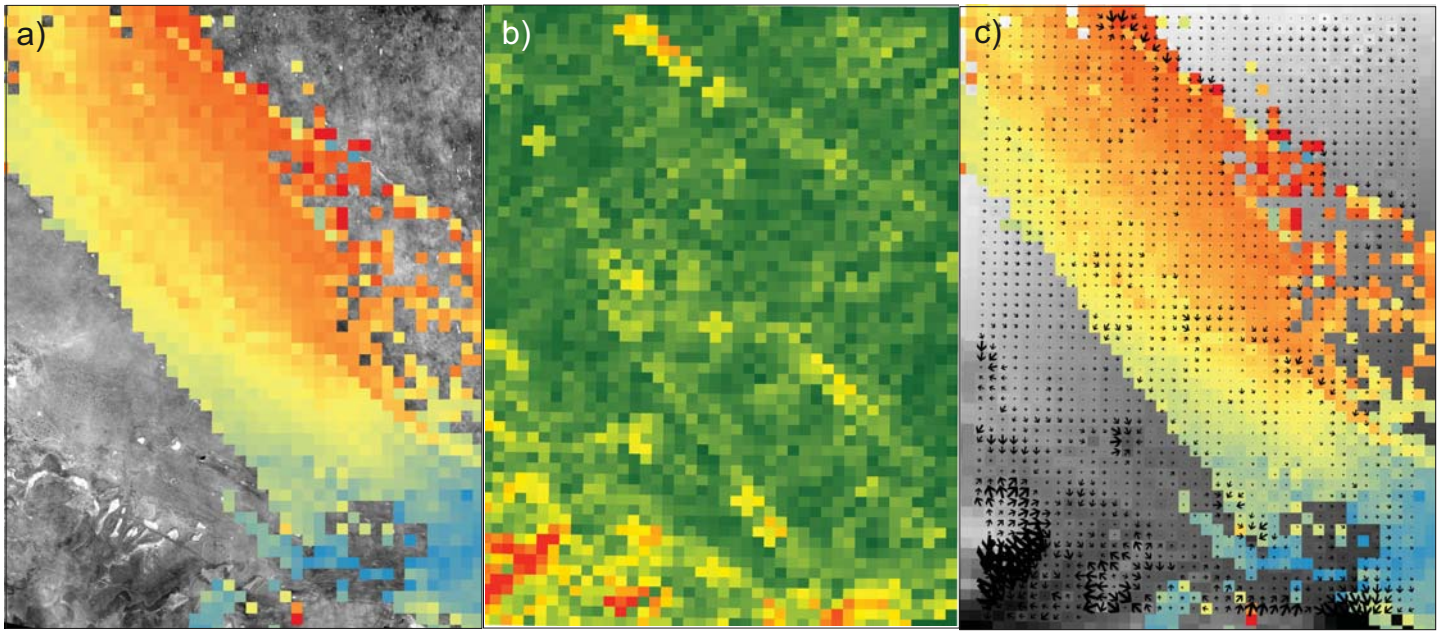
a)
b)
c)

Figure 4.

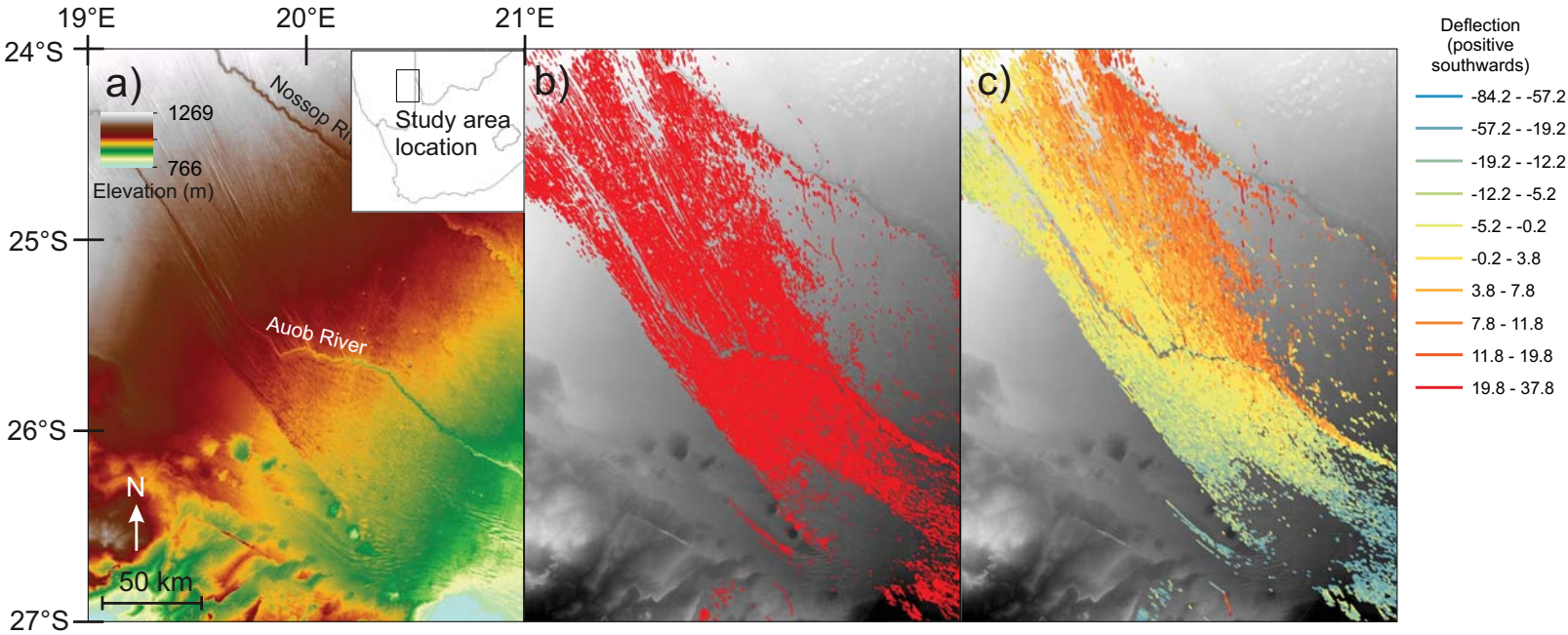
19°E
20°E
21°E
24°S
25°S
26°S
27°S
a)
b)
c)
1269
766
Elevation (m)
Nossop Ri
Study area
location
Auob River
N
50 km
Deflection
(positive
southwards)
-84.2 - -57.2
-57.2 - -19.2
-19.2 - -12.2
-12.2 - -5.2
-5.2 - -0.2
-0.2 - 3.8
3.8 - 7.8
7.8 - 11.8
11.8 - 19.8
19.8 - 37.8

Figure 5.

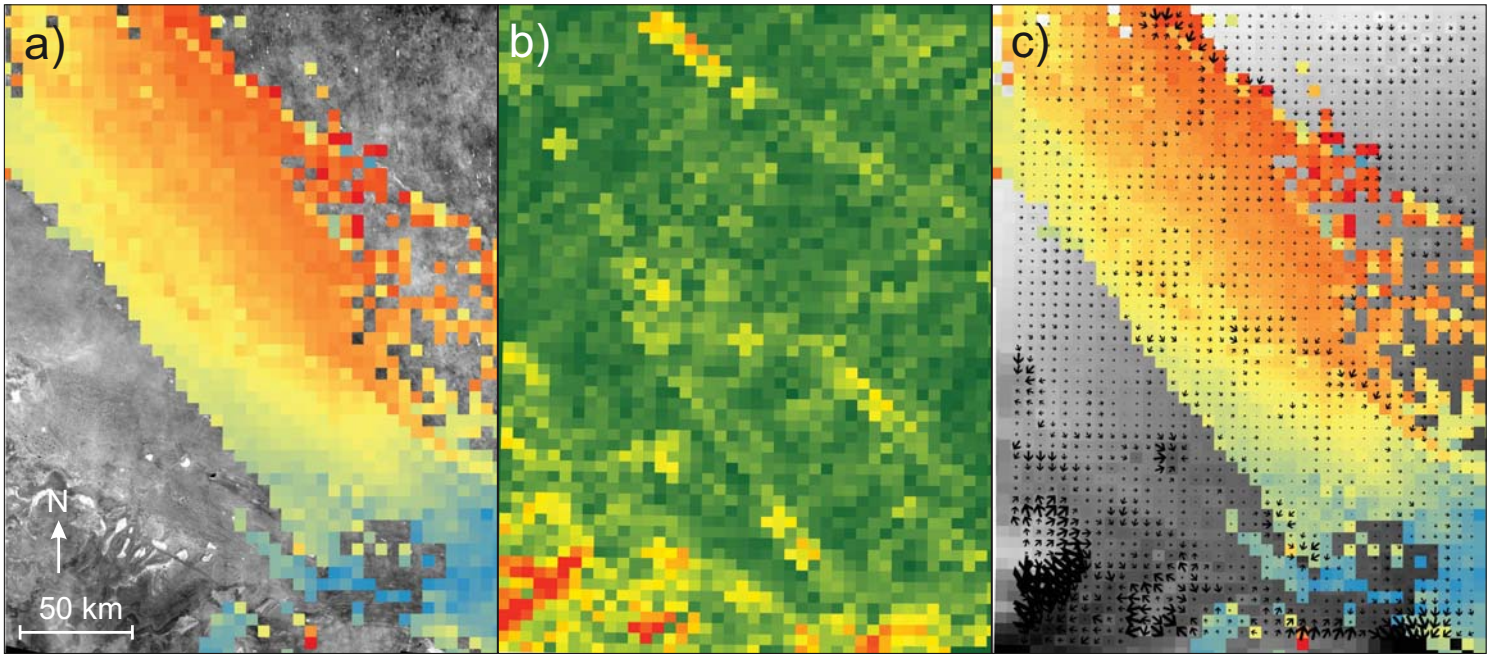
a)
b)
c)
N
50 km

Figure 6.

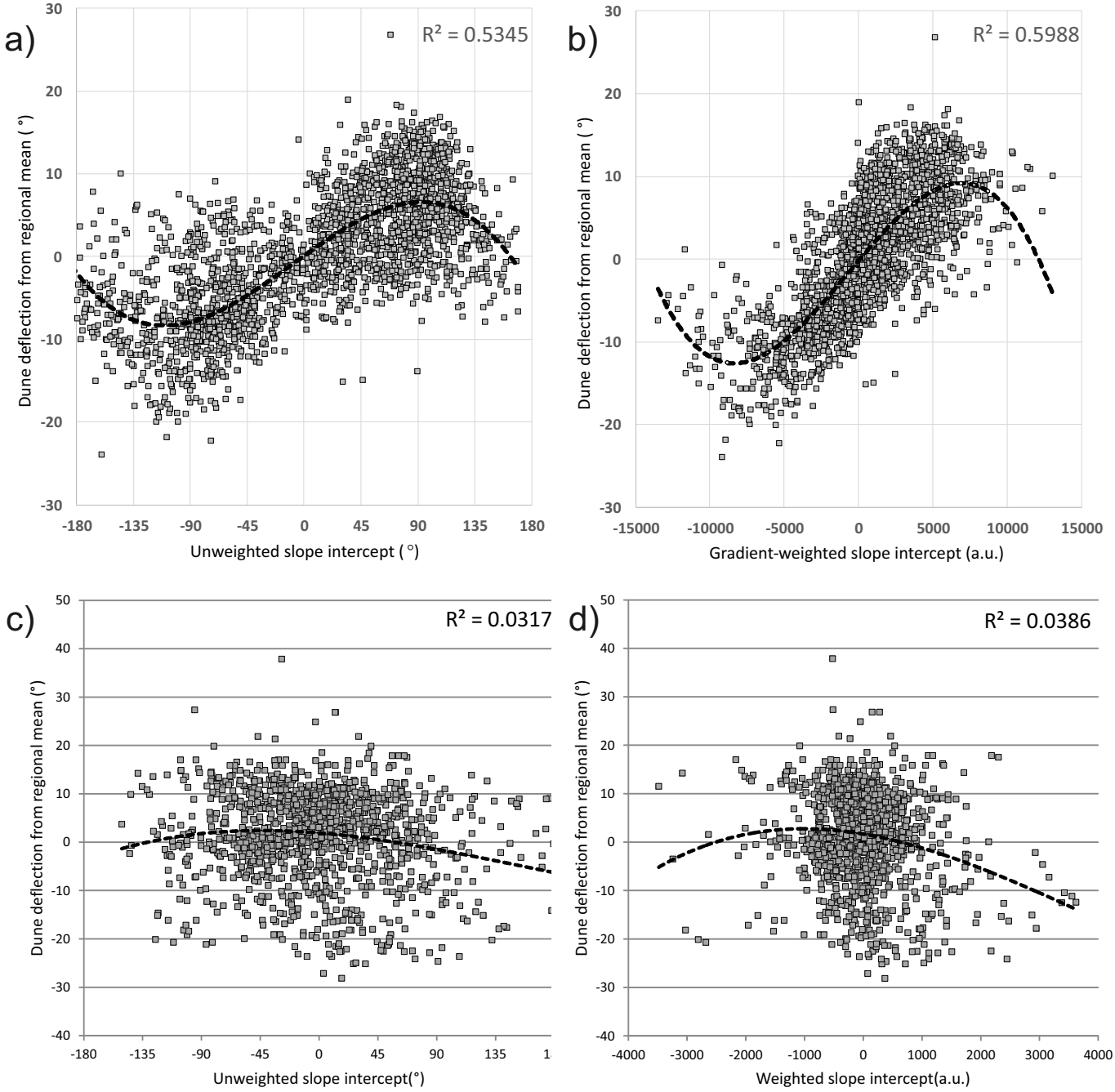
a)
R² = 0.5345
Dune deflection from regional mean (°)
Unweighted slope intercept (°)
b)
R² = 0.5988
Dune deflection from regional mean (°)
Gradient-weighted slope intercept (a.u.)
c)
R² = 0.0317
Dune deflection from regional mean (°)
Unweighted slope intercept(°)
d)
R² = 0.0386
Dune deflection from regional mean (°)
Weighted slope intercept(a.u.)

Figure 7.

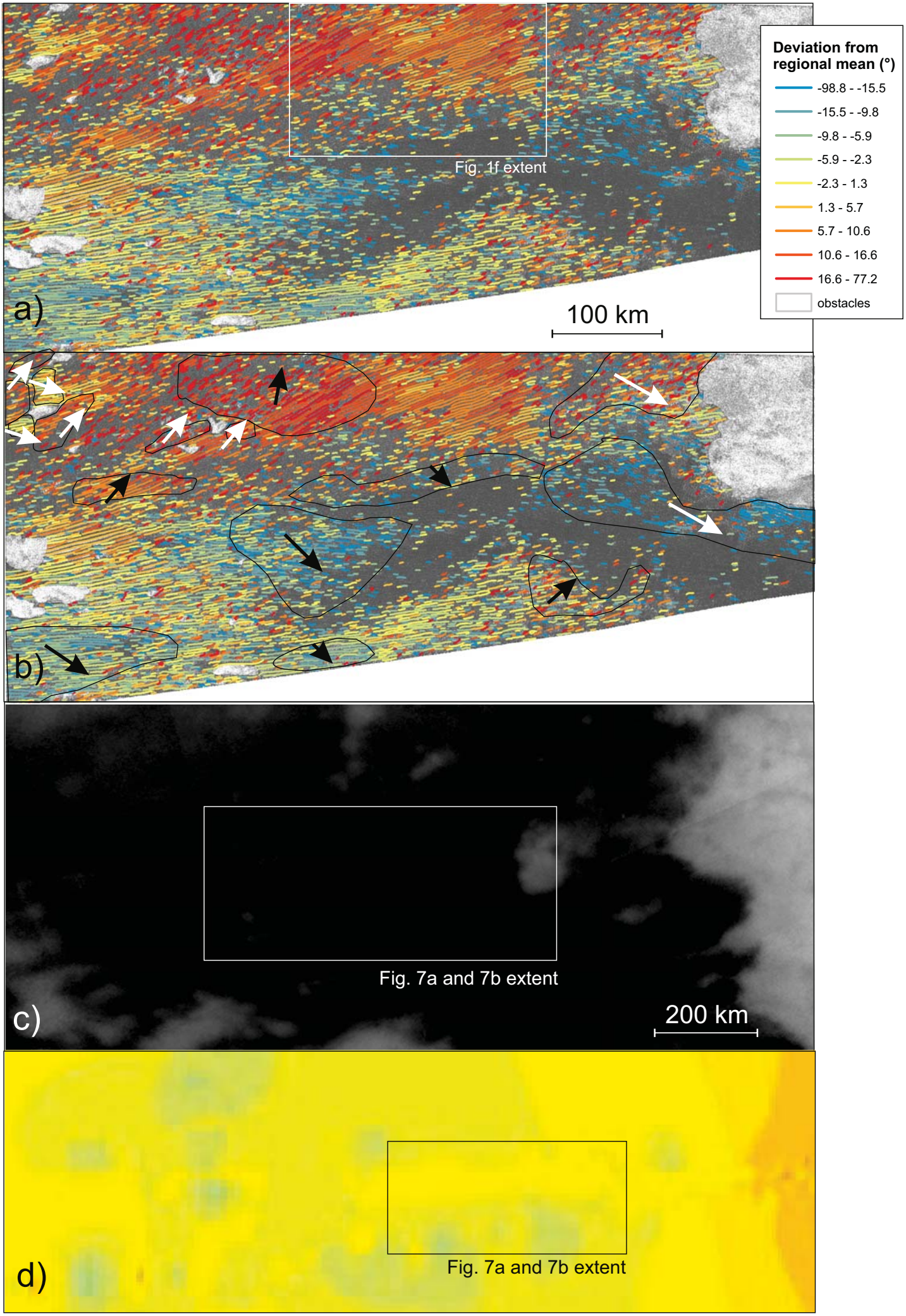
Deviation from regional mean (°)
-98.8 - -15.5
-15.5 - -9.8
-9.8 - -5.9
-5.9 - -2.3
-2.3 - 1.3
1.3 - 5.7
5.7 - 10.6
10.6 - 16.6
16.6 - 77.2
obstacles
Fig. 1f extent
a)
100 km
b)
Fig. 7a and 7b extent
c)
200 km
Fig. 7a and 7b extent
d)